IEEE Access
Multidisciplinary | Rapid Review | Open Access Journal

Received February 21, 2022, accepted March 7, 2022, date of publication March 10, 2022, date of current version March 21, 2022.

*Digital Object Identifier 10.1109/ACCESS.2022.3158621*

# Active and Reactive Power Control for Dual Excited Synchronous Generator in Wind Applications

**H. M. YASSIN, R. R. ABDEL-WAHAB, AND H. H. HANAFY**
Electrical Power Engineering Department, Faculty of Engineering, Cairo University, Giza 12613, Egypt
Corresponding author: H. M. Yassin (haitham.yassin@cu.edu.eg)

**ABSTRACT** This paper presents a dual excited synchronous generator (DESG) as a novel suitable alternative generation system for wind energy conversion systems. A new control strategy was proposed for the DESG wind turbine system. With this control technique, the DESG could be operated as a constant-speed constant-frequency (CSCF) generation system with the benefit of adjusting the reactive power or as a variable-speed constant-frequency (VSCF) generation system with the benefits of simple control methods and lower copper losses. Using the space phasor model of the DESG, a direct relationship between the electromechanical torque and the armature reactive power in terms of the field current space phasor magnitude and the field voltage space phasor angle is provided. The proposed control strategy is based on controlling the field-current space phasor magnitude and the field-voltage space phasor phase angle to regulate the active and reactive powers of the DESG. Simulation results, based on MATLAB/SIMULINK, for a 1.1 kW DESG wind turbine system have been executed to verify the introduced control technique under various operating conditions. Also, experimental studies have been carried out to validate the simulation results using the proposed control algorithm.

**INDEX TERMS** Wind energy conversion system, dual excited synchronous generator, reactive power control, maximum power point tracking.

## I. INTRODUCTION

Over the few last decades, the global demand for electrical energy has increased significantly due to the huge industrial development and population growth. As a result, traditional fossil fuel consumption has risen, resulting in many significant problems such as pollution, global warming, and the shortage of traditional fossil energy resources. To overcome these problems, there is a great interest in various areas of renewable energy resources as solar, wind, and hydropower [1], [2]. Wind energy has become one of the most rapidly growing renewable resources of electrical energy [3], [4]. As a result of wind energy attention, the overall capacity of wind energy installed worldwide by the end of 2020 reached 743 GW with an additional 93 GW of new wind power capacity [5].

There are many types of wind energy conversion systems (WECSs) that can be classified into three main groups based on wind turbine rotational speed,: fixed speed, limited variable speed, and variable speed [6].

Currently, variable-speed WECS has became the most commonly used technology owing to its benefits of maximum captured energy at diverse rotating speeds, reduced mechanical stress, reactive power control, and fewer voltage oscillations [7].

The most popular variable-speed wind energy conversion technologies are the doubly fed induction generator (DFIG) wind turbine system in addition to the direct-drive permanent magnet synchronous generator (PMSG) wind turbine system.

DFIG is considered the dominant among all WECSs because of its many merits such as the capability of variable speed operation over a wide range, the possibility of controlling active and reactive power independently, the capability of captureing maximum mechanical power, and its cost-effectiveness, where partially rated power electronic converters around 30 % of the generator rating are used [8]–[10]. Despite these advantages, DFIG has some disadvantages like frequent maintenance and additional electrical losses due to slip rings and brushes, also it is very sensitive to grid failures [11].

On the other hand, the advantages of higher efficiency, higher reliability, self-excitation, and lower required maintenance, make the PMSG with a full-power converter one of the

The associate editor coordinating the review of this manuscript and approving it for publication was Arturo Conde.

significant generators in the recent wind energy technology market [12], [13]. However it also suffers from the high cost of the PM, the cost of the fully rated converter and filters, and its demagnetization at high temperatures levels.

Recently, many developed generators have been presented for WECS like the brushless doublyfed induction generator (BDFIG) [14]–[16], as well as adual excited synchronous generator (DESG) [17], [18], stator-PM machines [19], which include like axial field flux-switching PM machines, doubly salient PM machine, and stator interior permanent magnet generators; and finally the flux modulated PM machines [20], [21] such as magnetic-geared PM machines, hybrid excited flux bidirectional modulated PM machines. Because of the absence of slip rings and brushes, BDFIG is advantageous for its high efficiency, high reliability, and low maintenance cost in comparison with DFIG. DESG can operate as a VSCF generating system as in WECS and hydroelectric power stations with very fluctuating heads.

DESG has been introduced in the literature as an important method for improving steady-state and dynamic stability, enhancing the reliability of the system, and controlling the active and reactive powers independently [22]–[24].

In [25]–[27], various analyses of DESG based on finite element models showed that the DESG is more stable and reliable than the conventional synchronous generator.

By using a suitable control method for DESG field voltages, terminal voltages with constant magnitude and frequency can be produced regardless in the variation of rotation speed [18]. It is known that the field windings must be excited by sinusoidal voltages at the slip frequency, and the phase sequence of the field voltages must be regulated so that the required terminal voltages frequency is equal to the sum of the frequency of the field voltages and the rotor rotational frequency.

Different control techniques have been introduced for DESG. In [28], an error signal depending on the difference between the terminal voltage and the desired value was used to determine the magnitude of the rquired excitation voltages, while the excitation voltage frequency was proportional to the rotor slip. In [29], a mathematical model of a DESG wind energy system with a novel control technique was introduced to maximize the total generated power and increase the efficiency of the machine. The proposed control technique depends on controlling the angle of the field-voltage space phasor, because efficiency may be expressed as a transcendental function of this angle. The simulation results proved that using the DESG with the proposed control algorithm can achieve a significant increase in the generated power compared with the standard induction machine.

Another control technique for DESG wind turbines was introduced in [30]. The proposed control algorithm aims to maximize the produced active power as well as actively regulate the active power flowing into the rotor to zero in the supersynchronous operation region. Controlling of the rotor power, according to this control technique, leads to the possibility of replacing the back-to-back converter of the grid-side converter (GSC) with a simple unregulated rectifier leading to a decrease in cost as well as increase in system reliability.

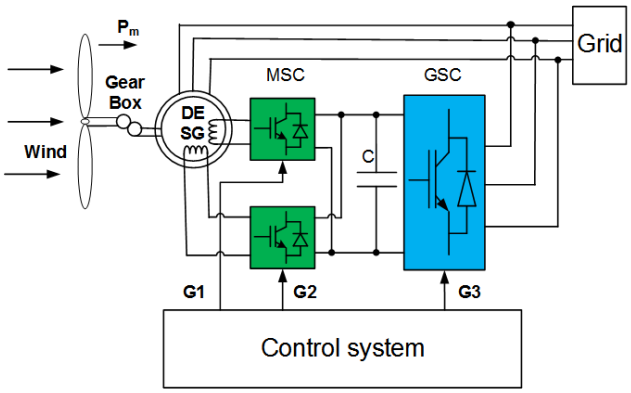


**FIGURE 1.** Schematic of DESG wind turbine system.

In comparison with the DFIG, the DESG can operate in low-speed wind applications using a low gearbox ratio due to the facility of designing large number of poles and a better simplicity of the control techniques, because the magnetic axes of the field windings are normally decoupled [30]. The presence of two-field winding made the DESG capable of operating as a CSCF generation system with the benefit of adjusting the reactive power or a VSCF generating system such as the DFIG with the benefits of easier control, lower copper loss, and higher efficiency [31].

In this work, a DESG-based wind turbine system is examined with a new control strategy to maximize the capture mechanical power for each wind speed, as well as to regulate the reactive power injected to the grid, when used as a CSCF generation system. It is possible to achieve these objectives by selecting a proper control technique for the excitation field currents. Based on the system mathematical model, the electromechanical torque, as well as the armature reactive power, can be derived in terms of the field-current space phasor magnitude and the field-voltage space phasor phase angle. The magnitude of the space phasor of the field current is used to control the electromechanical torque and hence control the generated active power, whereas the armature reactive power is regulated by the angle of the field voltage space phasor. To verify the introduced control technique, simulation of a 1.1 kW DESG wind turbine system based on MATLAB/Simulink was used. Finally, to confirm the simulation results, experimental results were obtained.

This paper is a revised and expanded version of the conference paper given in [32].

This paper is prepared as follows: in section II, the modelling of the DESG based wind turbine system is derived. In section III, the main principle of the applied control strategy is demonstrated. Section IV presents the simulation results as well as its discussion. Section V presents the experimental results. Finally, the conclusions are presented in Section VI.

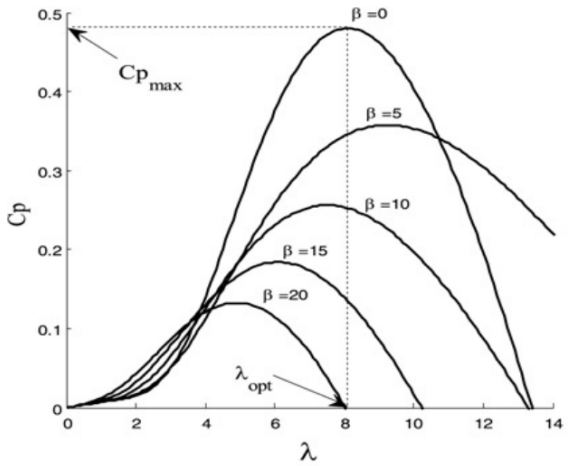


**FIGURE 2.** Cp–λ curve for different pitch angles.

## II. MODELLING OF DESG WIND ENERGY CONVERSION SYSTEM

The configuration of the DESG wind energy conversion system is shown in Fig. 1. In this scheme, the DESG is connected to the turbine via a gearbox, while the armature terminals are directly connected to the grid, and the field windings are fed through a back-to-back converter. The back-to-back method is important for the DESG to allow bidirectional power flow into the field side.

### A. MODELLING OF WIND TURBINE

The extracted mechanical power from the wind turbine can be written in the following equation [6]:

$$P_t = \frac{1}{2}\rho\pi R^2 C_p(\lambda, \beta) V_w^3 \tag{1}$$

where $P_t$ is the wind's extracted mechanical power (W), $\rho$ is the density of air (kg/m$^3$), R is the turbine blade's radius (m), $V_w$ is the wind speed (m/s), and $C_p$ is the power conversion coefficient, which is a function of the blade pitch angle $\beta$ (deg.) and tip-speed ratio $\lambda$ (TSR).

The TSR can be calculated using wind speed and the turbine's rotational angular rotor speed.

$$\lambda = \frac{\omega_t R}{V_w} \tag{2}$$

where $\omega_t$ is the turbine's rotational angular speed (rad/sec), which is related to the generator's rotational angular speed $\omega_m$ and the gearbox ratio (GR) by

$$\omega_m = \omega_t \, GR \tag{3}$$

Fig. 2 shows the ($C_p$–$\lambda$) characteristics for various values of the pitch angle $\beta$. Where the maximum value of $C_p$ is occurred at $\lambda_{opt}$ and $\beta = 0°$, and hence the maximum power of the turbine is found at a point of $\lambda_{opt}$ and $C_{p\_max}$.

### B. MATHEMATICAL MODEL OF DESG

The construction of the DESG under study differs from that of conventional synchronous generators due to the presence of two field windings instead of one. Fig. 3 illustrates the schematic of DESG having two non-identical field windings with orthogonal magnetic axes, while the armature has symmetrical three-phase windings.

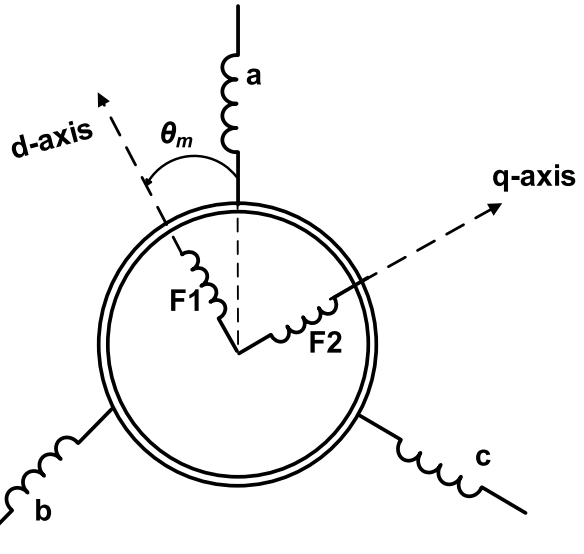


**FIGURE 3.** Schematic of DESG.

It is conceivable to derive the analytical model of the DESG in the rotor reference frame under assumptions of neglecting the iron and mechanical losses, neglecting the core saturation, assuming a cylindrical rotor machine and sinusoidal air gap MMF as follows:

$$\vec{V}_{ds} = -R_s\vec{I}_{ds} - L_s\frac{d\vec{I}_{ds}}{dt} + \omega_m L_s\vec{I}_{qs} + L_m\frac{d\vec{I}_{f1}}{dt} - \omega_m L_m\vec{I}_{f2} \tag{4}$$

$$\vec{V}_{qs} = -R_s\vec{I}_{qs} - L_s\frac{d\vec{I}_{qs}}{dt} - \omega_m L_s\vec{I}_{ds} + \omega_m L_m\vec{I}_{f1} + L_m\frac{d\vec{I}_{f2}}{dt} \tag{5}$$

$$\vec{V}_{f1} = R_{f1}\vec{I}_{f1} + L_{f1}\vec{I}_{f1} - L_m\frac{d\vec{I}_{ds}}{dt} \tag{6}$$

$$\vec{V}_{f2} = R_{f2}\vec{I}_{f2} + L_{f2}\vec{I}_{f2} - L_m\frac{d\vec{I}_{qs}}{dt} \tag{7}$$

$$\theta_m = \int \omega_m dt \tag{8}$$

The voltage and current could be written in space phasor form as follows:

$$\vec{V}_s = V_s e^{j(\omega_s t - \theta_m)} = \vec{V}_{ds} + j\vec{V}_{qs} \tag{9}$$

$$\vec{I}_s = I_s e^{j(\omega_s t - \theta_m - \varphi_s)} = \vec{I}_{ds} + j\vec{I}_{qs} \tag{10}$$

$$\vec{V}_f = V_f e^{j(\omega_s t - \theta_m + \gamma)} = \vec{V}_{f1} + j\vec{V}_{f2} \tag{11}$$

$$\vec{I}_f = I_f e^{j(\omega_s t - \theta_m + \gamma - \varphi_r)} = \vec{I}_{f1} + j\vec{I}_{f2} \tag{12}$$

where, the armature and field-voltages space vectors in the rotor frame are $\vec{V}_s$ and $\vec{V}_f$, respectively. $\vec{I}_s$ and $\vec{I}_f$ are the armature and field currents space vectors in the rotor frame, respectively. $V_{ds}$ and $V_{qs}$ are the d and q-axis components of the stator voltage. $I_{ds}$ and $I_{qs}$ are the d and q-axis components of the stator current. $R_s$ and $L_s$ are the resistance and self-inductance of the armature winding per phase, while $R_{f1}$, $R_{f2}$,

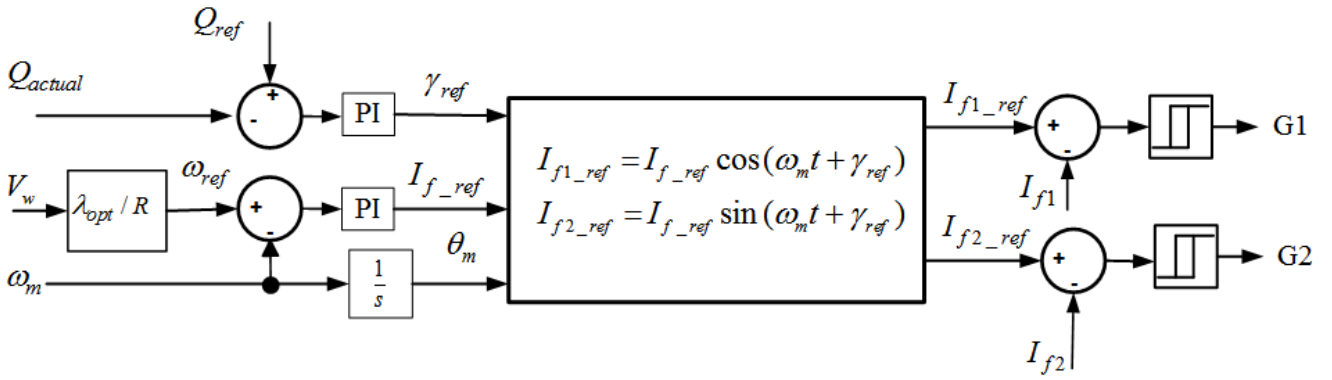


**FIGURE 4.** Schematic diagram of the presented control technique for MSC.

$L_{f1}$, and $L_{f2}$ are the resistances and self-inductances of the field windings referred to the stator winding, and $L_m$ is the mutual inductance of the machine. While $\omega_s$ is the angular frequency of the armature voltage, $\theta_m$ is the angular position of the rotor frame with respect to the armature frame, $\Phi_s$ and $\Phi_r$ are the armature and field impedance angle, respectively, and $\gamma$ is the angle of field voltage space vector with respect to armature voltage space vector. The electromagnetic torque, as well as the active and reactive powers of the armature can be expressed as a function of the space phasors of the voltage and currents, as follows:

$$T_{em} = pL_m \mathrm{Im}\left(\vec{I}_s \vec{I}_f^{\,*}\right) \tag{13}$$

$$P_s = \mathcal{R}\left(\vec{V}_s \vec{I}_s^{\,*}\right) \tag{14}$$

$$Q_s = \mathrm{Im}\left(\vec{V}_s \vec{I}_s^{\,*}\right) \tag{15}$$

where, p is the number of pole pairs, $\mathcal{R}$ (x) and Im (x) are the real and imaginary parts of the complex number ($x$), and * is the conject operator.

Then, the system mechanical equation is given as

$$T_t - T_{em} = J\frac{d\omega_m}{dt} + B_m\omega_m \tag{16}$$

where $T_t$ is the turbine torque, $T_{em}$ is the electromechanical torque, J is the moment of inertia, and $B_m$ is the viscous friction constant.

## III. CONTROL TECHNIQUE

The possibility of obtaining the maximum productive energy despite the change in wind speed is considered one of the most important merits of usingDESG in wind generation systems. This can be efficiently performed by selecting an appropriate control method for the excitation currents. The field windings must be fed with a current of frequency proportional to the slip speed. In the DSEG wind energy conversion system, the two field windings are fed through two single-phase converters to control the injection of active and reactive power into the grid. These converters are called machine-side converters (MSC) which are supplied through the DC link as presented in Fig. 1, while the GSC maintains a constant desired value for the DC link voltage.

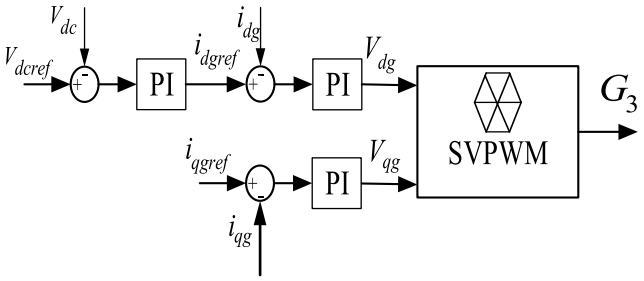


**FIGURE 5.** Schematic diagram of the control technique for GSC.

### A. MACHINE SIDE CONVERTERS CONTROL

Analysis the DESG mathematical model under steady-state operating conditions proved that the field current parameters can be used to express the electromechanical torque as well as the armature reactive power as given in (17) and (18).

The armature reactive power and electromechanical torque are dependent on the field-current space phasor magnitude and the field-voltage space phasor phase angle ($\gamma$). However, these two parameters simultaneously affect on the electromechanical torque and reactive power. Fig. 4 illustrates a schematic diagram of the proposed control strategy.

In the introduced control strategy, the field-current space phasor magnitude is used to control the electromechanical torque to maximize the captured mechanical power from the wind. On the other hand, the armature reactive power is controlled through the phase angle of the field-voltage space phasor. The output signals G1 and G2 are the gate signals of the two single-phase converters of the field windings as shown in Figure 1.

$$T_{em} = \frac{pR_s V_s L_m}{R_s^2 + \omega_s^2 L_s^2} I_f \sin(\gamma - \varphi_r) + \frac{p\omega_s V_s L_s L_m}{R_s^2 + \omega_s^2 L_s^2} I_f \cos(\gamma - \varphi_r) + \frac{pRs\omega_s L_m^2}{R_s^2 + \omega_s^2 L_s^2} I_f^2 \tag{17}$$

$$Q_s = \frac{\omega_s^2 V_s L_s L_m}{R_s^2 + \omega_s^2 L_s^2} I_f \sin(\gamma - \varphi_r) + \frac{R_s\omega_s V_s L_m}{R_s^2 + \omega_s^2 L_s^2} I_f \cos(\gamma - \varphi_r) + \frac{\omega_s L_s V_s^2}{R_s^2 + \omega_s^2 L_s^2} \tag{18}$$

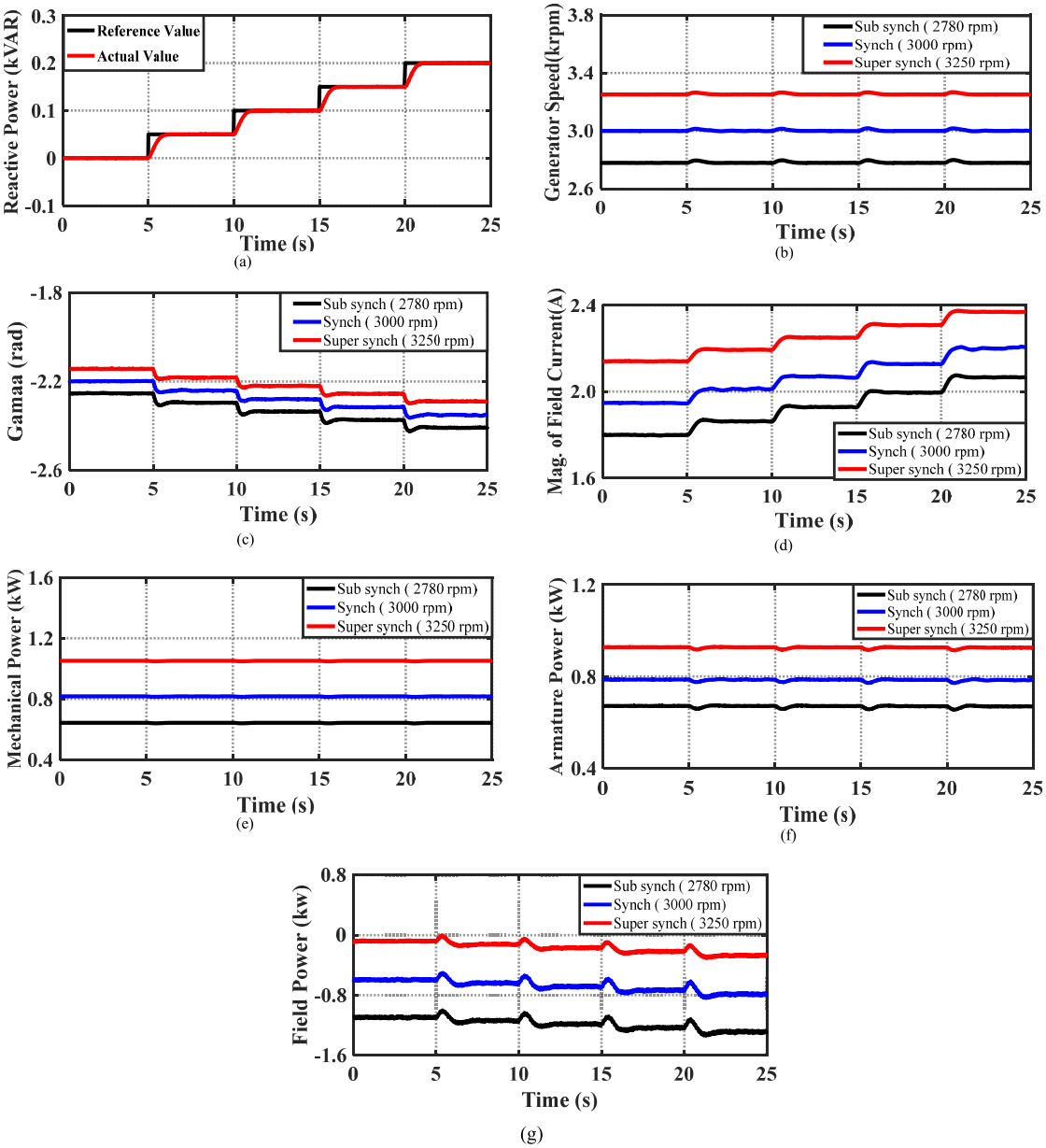


**FIGURE 6.** Simulation results for step changes in armature reactive: (a) Armature reactive power response and its reference, (b) Generator rotational speed, (c) phase angle ($\gamma$), (d) Amplitude of the current space vector, (e) Mechanical power response, (f) Armature power response, (g) Field power response.

### B. GRID SIDE CONVERTER CONTROL

The main purpose of the GSC is to regulate the DC-link voltage at a constant level. A field-oriented control algorithm was used to perform this function. Fig. 5 shows a proposed layout for this algorithm. In this algorithm, the d-axis component of the grid current ($i_{dg}$) was used to maintain the DC-link voltage at a constant value. On the other hand, the q-axis current ($i_{qg}$) was set to zero to confirm zero rotor-reactive power. Therefore, any reactive power exchange is perform only over the armature side, thereby reducing the power converters.

## IV. SIMULATION RESULTS

To validate the effectiveness of the proposed control technique, the analytical model in the previous section was simulated using MATLAB/SIMULINK for a 1.1 kW DESG wind turbine. Appendix A presents the DESG-based WECS parameters used for the simulation. The proposed scheme is verified with two different cases: the first case is constant-speed operation, and the other case is variable-speed operation.

### A. CASE 1: CONSTANT SPEED OPERATION

The proposed control technique was tested for a step change in the armature reactive power at three different values of wind speed individually as shown in Fig. 6. The proposed controller succeeded in regulating the step changes in reactive power to its desired reference value as shown in Fig. 6(a). The rotating speed of the generator is constant and accurately

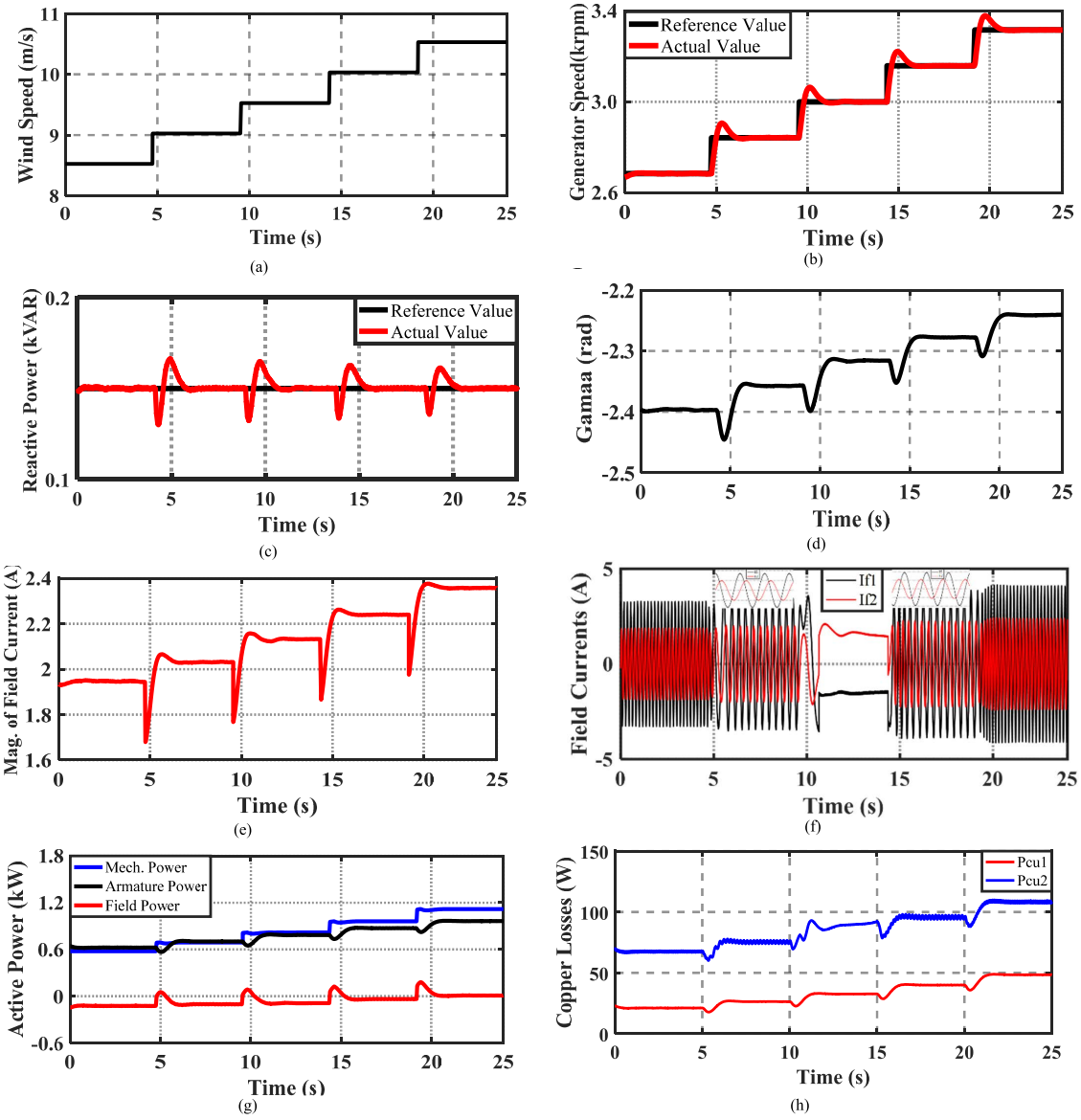


**FIGURE 7.** Simulation results for step changes in wind speed: (a) Wind speeds, (b) Generator rotational speed, (c) Armature reactive power response, (d) Field voltage space phasor angle ($\gamma$), (e) Field current space phasor magnitude, (f) Field Current response, (g) Active power response, (h) Armature and field copper losses.

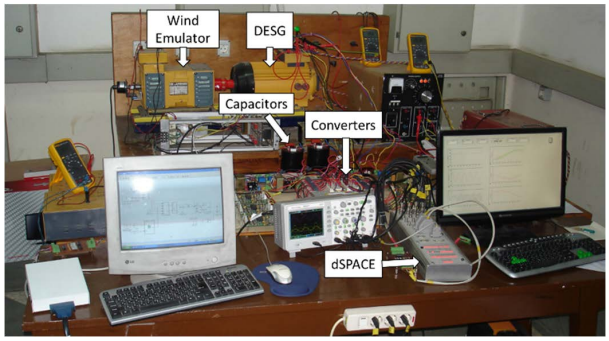


**FIGURE 8.** The hardware setup layout.

aligned with its desired values as indicated in Fig. 6(b). The control actions are shown in Fig. 6(c) and Fig. 6(d). The field voltage angle was controlled to trace the variation in the generated armature reactive power. Simultaneously, the field voltage space vector amplitude should be varied to eliminate the effect of the phase angle variation on the electromechanical torque. Therefore, the rotation speed was maintained at its reference value. As illustrated in Fig. 6(e) and Fig. 6(f); the captured mechanical and the generated armature active powers have constant values at each operating speed condition because the rotational speed is constant. From Fig. 6(g); it could be noticed that the field power is changed with each variation of reactive power since it is dependent on the field currents.

### B. CASE 2: VARIABLE SPEED OPERATION

On the other hand, the simulation results were obtained in the case of step variations of wind speed while maintaining the armature reactive power constant as shown in Fig. 7.

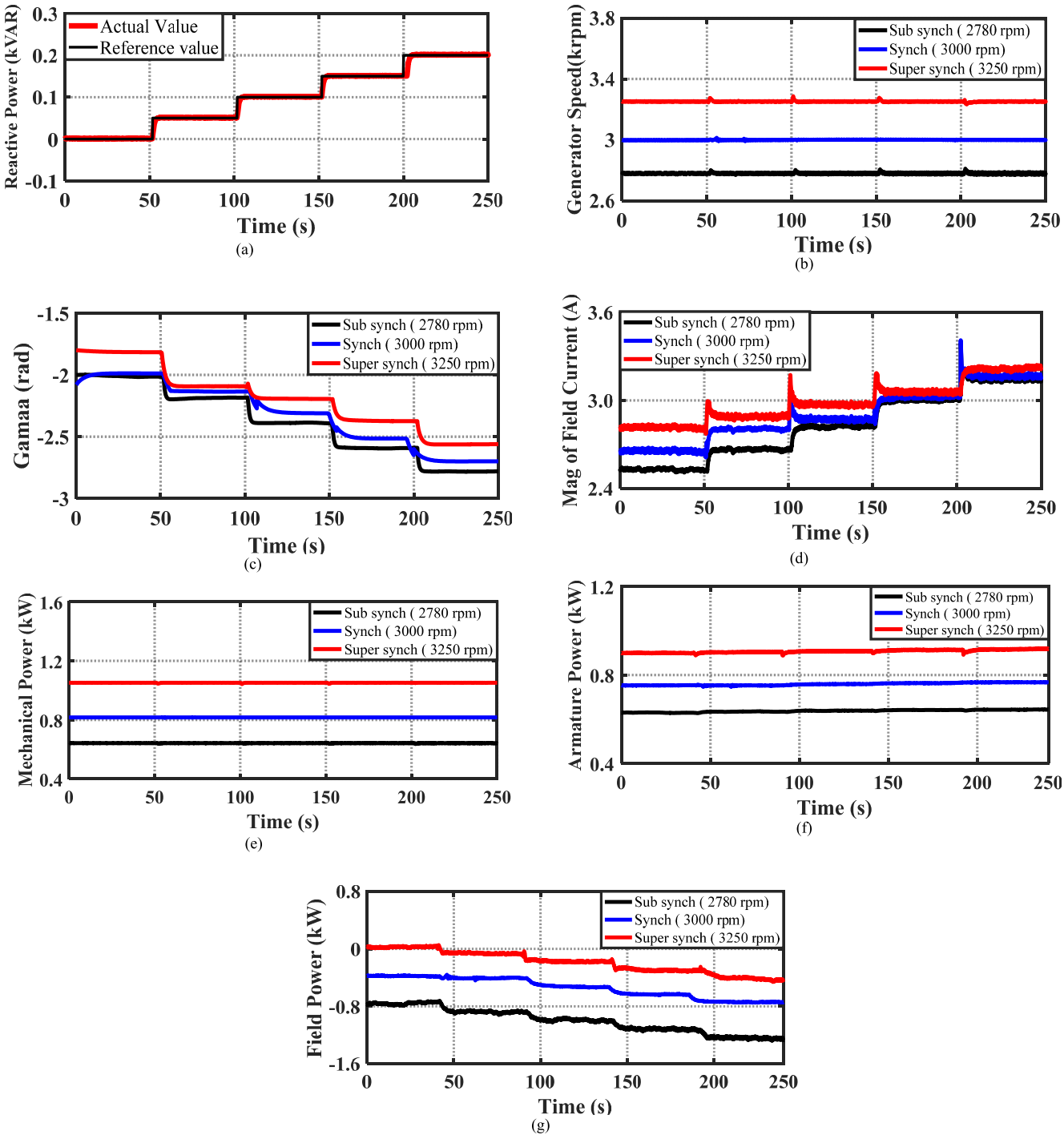


**FIGURE 9.** Experimental results for step changes in the armature reactive: (a) Armature reactive power response and its reference, (b) Generator rotational speed, (c) phase angle ($\gamma$), (d) Amplitude of the current space vector, (e) Mechanical power response, (f) Armature power response, (g) Field power response.

In this situation, the armature reactive power is maintained at 150 VAR whereas the active power changes with wind speed variation to achieve MPPT. The profile of the tested wind speeds is shown in Fig. 7 (a). As seen in Fig. 7 (b), the introduced controller regulates the generator speed to track wind speed variations according to the MPPT technique. Fig. 7 (c) shows that the armature reactive power is constant and exactly aligned with its reference value. The control actions are shown in Fig. 7 (d) and Fig. 7 (e). To achieve MPPT, the field-current space phasor is modified according to the required reference generator speed. Simultaneously, the control system adjusts the angle of the field voltage space phasor to compensate for the armature reactive power effect of the amplitude of the field current space phasor

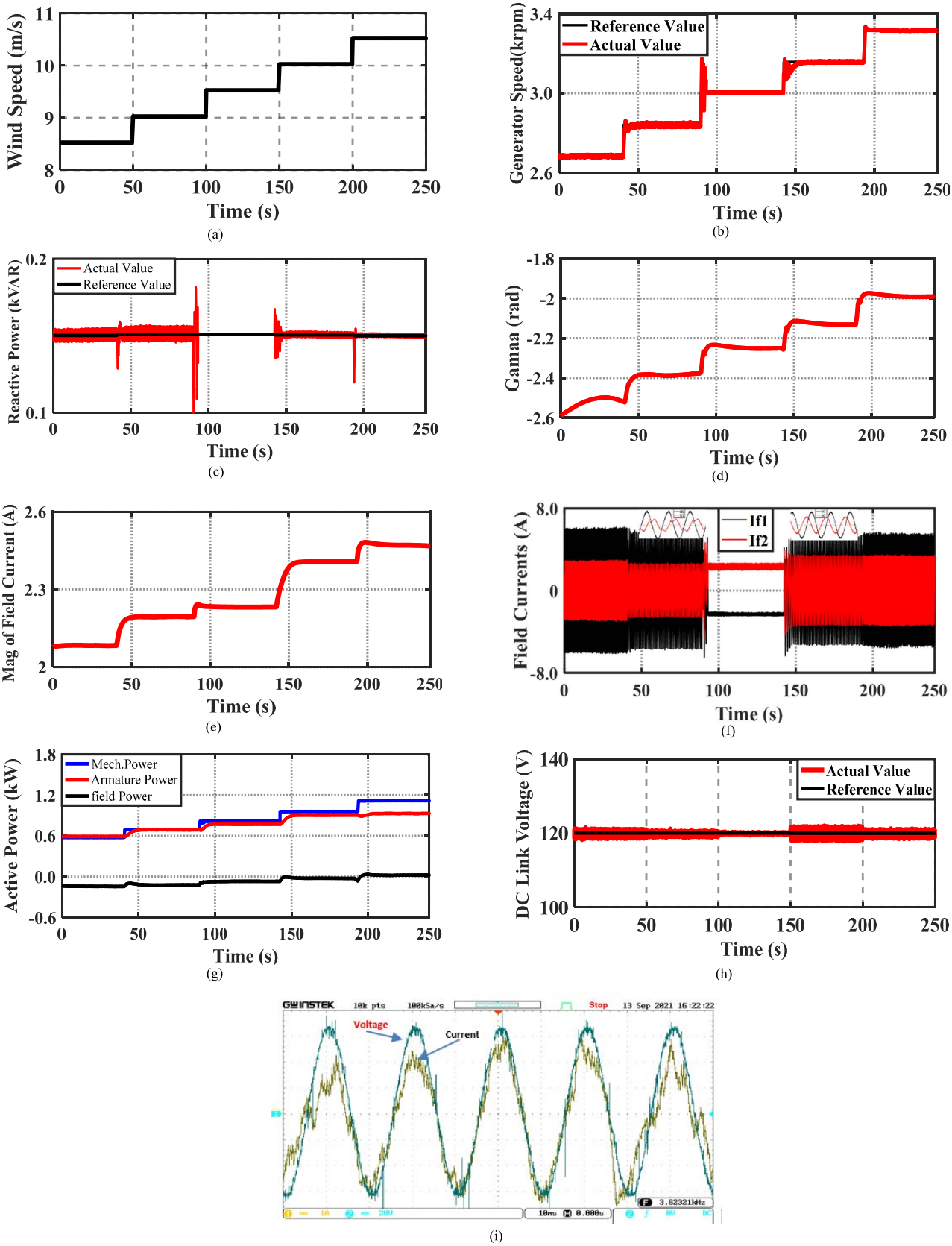


**FIGURE 10.** Experimental results for step changes in wind speed: (a) Wind speeds, (b) Generator rotational speed, (c) Armature reactive power response, (d) phase angle ($\gamma$), (e) Magnitude of the field current space vector, (f) Field Current response, (g) Active power response, (h) DC link voltage response, (i) the voltage and current of phase A of the GSC.

**TABLE 1.** The simulation results for variable speed operation.

| Wind Speed (m/s) | 8.5 | 9 | 9.5 | 10 | 10.5 |
|---|---|---|---|---|---|
| Generator speed (rpm) | 2685 | 2840 | 3000 | 3160 | 3315 |
| Mechanical Power (W) | 580 | 688 | 817 | 960 | 1115 |
| Armature power(W) | 620 | 702 | 785 | 873 | 965 |
| Field power(W) | -134 | -123 | -90 | -47 | -3 |
| Armature copper losses(W) | 21 | 26 | 33 | 40 | 48 |
| Field copper losses(W) | 73 | 83 | 89 | 94 | 105 |
| Efficiency (%) | 83.8 | 84.2 | 85.1 | 86.0 | 86.3 |

variation on the armature reactive power. Fig. 7 (f) shows the time variation of field currents. Because the generator speed changes with the wind speed, the controller changed the phase sequence and values of the field currents to extract maximum power. These currents have a phase shift of 90°, but their amplitudes are different because the field windings are non-identical. It can be noticed that the field currents have a slip frequency corresponding to the operating speed. When the generator speed was changed from sub-synchronous to super-synchronous, the sequence of the two filed currents was reversed. The active power of the wind turbine, armature, and field are shown in Fig. 7 (g). The MPPT algorithm controls the armature active power to track the maximum extracted mechanical power at each wind speed. It can be noted that, during sub-synchronous speed operation, the armature power is greater than the mechanical power because a part of the field power is transferred to the armature by induction. The negative sign of the field power indictes that the field circuit absorbed the active power from the grid. Fig. 7(h) shows the copper losses of the armature ($P_{cu1}$) and field ($P_{cu2}$). Table 1 summarizes the system efficiency over the entire speed range.

## V. EXPERIMENTAL RESULTS

To validate the simulation results experimentally, the laboratory setup, shown in Fig. 8, was used. Where a 1.3 kW separately excited DC motor is used as a turbine emulator and coupled to a 1.1 kW DESG. The armature terminals of the DESG are connected to the grid directly. On the other hand, the field windings are connected to the grid through two power converters, MSC and GSC with DC-link connecting between the two converters. The DC link consists of two series 6800 $\mu$F capacitors with a mid-point that is connected to the neutral point of the field windings of the generator. The GSC was controlled via a data acquisition card, while the control of MSC is implemented through the dSPACE DS1104 R&D controller. The switching frequency is 5 kHz. Appendix A lists the parameters ysed for the DESG and DC motor. Similarly, as in the simulation section, the system was examined experimentally for two different cases.

### A. CASE 1: CONSTANT SPEED OPERATION

Fig. 9 represents the experimental results for step changes in the injection armature reactive power at three different wind speeds. Fig. 9 (a). shows the step variation of the armature reactive power. As demonstrated in Fig. 9 (b), the generator operating speeds were constant at their reference values. The response of the field voltage space phasor angle and the field current space phasor magnitude are regulated to trace the variation of the armature reactive power as shown in Fig. 9 (c) and Fig. 9 (d). The captured mechanical and the generated armature powers are constant at each operating speed, as shown in Fig. 9 (e) and Fig. 9 (f). because the field power is dependent on the field currents, it changes with each variation in reactive power as shown in Fig. 9 (g).

It is clear that there is a small difference between the control action values (the field-voltage space phasor angle and the field-current space phasor magnitude) in the simulation and experimental results. This difference could be the result of the assumptions made during the simulation.

### B. CASE 2: VARIABLE SPEED OPERATION

Fig. 10 shows the experimental results of variable speed operation at a constant reactive power. Fig. 10(a). depicts the shpe of the wind speed. Fig. 10(b) shows that the actual generator speed tracks its optimal reference value to capture the maximum generated power in the wind turbine emulator at each step in the wind speed. Fig. 10(c) shows the response of the injection reactive power to the grid. The control actions are shown in Fig. 10(d) and Fig. 10(e). Fig. 10(f) shows the response of the injected field currents. It is clear that, the controller varies the amplitude, phase shift, and frequency of the injected field currents in response to the operating wind speed. Based on this, in the synchronous speed operating zone, the field currents are DC. The active powers of the turbine, armature, and field are shown in Fig. 10(g). The direction of field power is reversed in some super-synchronous speed regions, as can be seen. The response of the DC-link voltage is shown in Fig. 10(h), and it is constant at its reference value of 120V. Fig. 10(i) shows the voltage and current of phase A of the grid side converter. The phase shift between the voltage and current is zero, as can be shown. Thus, no reactive power is exchanged between the field side and the grid, as all reactive power passes through the armature side. Fig. 10(h) and Fig. 10(i) confirm the success of the proposed control technique of the GSC in achieving its main objectives.

## VI. CONCLUSION

This paper introduces a novel control technique for a DESG wind energy conversion system. A complete mathematical model of the entire system with the proposed control strategy was derived in the rotor reference frame to study system performance.

The main purpose of the proposed control strategy is to control the field voltage and current parameters to obtain the maximum captured mechanical power from the wind and

to control the injection reactive power to the grid. In this strategy, the generated active power is controlled by the magnitude of the space phasor of the field-current, whereas the injection reactive power is controlled through the phase angle of the field voltage space phasor.

Simulation and experimental results for a small-scale DESG wind turbine energy conversion system were performed to verify the proposed control technique. The obtained results revealed a good correlation between the experimental and simulation results. Consequently, using the proposed control strategy, the DESG is capable of controlling the injection of reactive power to the grid in addition to tracking the wind maximum power when operating at either constant speed or variable speed modes. Hence, according to the obtained results, one can conclude that the DESG is a promising alternative for generators used in WECSs.

## APPENDIX

See Tables 2–4.

**TABLE 2. Wind turbine parameters.**

| Parameter | Value |
|---|---|
| Rated mechanical power of wind turbine | 1.1 kW |
| Cpmax | 0.376478 |
| $\lambda_{opt}$ | 5.03808 |
| Rated wind speed | 10.5 m/s |
| Turbine blade radius | 1.1 m |

**TABLE 3. Parameters of DESG.**

| Parameter | Value |
|---|---|
| Nominal power | 1.1 kW |
| Nominal frequency | 50 Hz |
| Nominal line voltage | 380 V |
| Pairs poles | 2 |
| Resistance of armature winding ($R_s$) | 4.65 Ω |
| Resistance of the first field winding ($R_{f1}$) | 4.7 Ω |
| Resistance of the second field winding ($R_{f2}$) | 9.4 Ω |
| Self- inductance of armature winding ($L_s$) | 0.5330 mH |
| Mutual inductance | 518 mH |
| Self-inductance of the first field winding ($L_{f1}$) | 0.5405 mH |
| Self-inductance of the second field winding ($L_{f2}$) | 1.599 mH, |
| Moment of inertia | 0.0108 kg.m$^2$ |

**TABLE 4. Parameters of separately excited DC motor.**

| Parameter | Value |
|---|---|
| Rated Power | 1.1 kW |
| Rated Voltage of Armature | 440 V |
| Rated Voltage of Field | 190 V |
| Rated Current of Armature windings | 3.6 A |
| Rated Current of Field windings | 0.6 A |
| No of Poles | 2 |

## REFERENCES


[1] Y. M. Alsmadi, L. Xu, F. Blaabjerg, A. P. Ortega, and A. Wang, "Comprehensive analysis of the dynamic behavior of grid-connected DFIG-based wind turbines under LVRT conditions," in *Proc. IEEE Energy Convers. Congr. Exposit. (ECCE)*, Sep. 2015, pp. 4178–4187.

[2] E. Y. Bitar, R. Rajagopal, P. P. Khargonekar, K. Poolla, and P. Varaiya, "Bringing wind energy to market," *IEEE Trans. Power Syst.*, vol. 27, no. 3, pp. 1225–1235, Aug. 2012.

[3] G. Gualtieri, "A comprehensive review on wind resource extrapolation models applied in wind energy," *Renew. Sustain. Energy Rev.*, vol. 102, pp. 215–233, Mar. 2019.

[4] Z. Zeng, H. Yang, R. Zhao, and C. Cheng, "Topologies and control strategies of multi-functional grid-connected inverters for power quality enhancement: A comprehensive review," *Renew. Sustain. Energy Rev.*, vol. 24, pp. 223–270, Aug. 2013.

[5] J. Lee and F. Zhao, "GWEC global wind report," *Wind Energy Technol.*, to be published. [Online]. Available: www.gwec.net

[6] M. Cheng and Y. Zhu, "The state of the art of wind energy conversion systems and technologies: A review," *Energy Convers. Manage.*, vol. 88, pp. 332–347, Dec. 2014.

[7] M. Liserre, R. Cardenas, M. Molinas, and J. Rodriguez, "Overview of multi-MW wind turbines and wind parks," *IEEE Trans. Ind. Electron.*, vol. 58, no. 4, pp. 1081–1095, Apr. 2011.

[8] M. Yin, Y. Xu, C. Shen, J. Liu, Z. Y. Dong, and Y. Zou, "Turbine stability-constrained available wind power of variable speed wind turbines for active power control," *IEEE Trans. Power Syst.*, vol. 32, no. 3, pp. 2487–2488, May 2017.

[9] I. Ngamroo, "Review of DFIG wind turbine impact on power system dynamic performances," *IEEJ Trans. Electr. Electron. Eng.*, vol. 12, no. 3, pp. 301–311, May 2017.

[10] G. S. Kaloi, J. Wang, and M. H. Baloch, "Active and reactive power control of the doubly fed induction generator based on wind energy conversion system," *Energy Rep.*, vol. 2, pp. 194–200, Nov. 2016.

[11] A. M. S. Yunus, A. Abu-Siada, M. A. S. Masoum, M. F. El-Naggar, and J. X. Jin, "Enhancement of DFIG LVRT capability during extreme short-wind gust events using SMES technology," *IEEE Access*, vol. 8, pp. 47264–47271, 2020.

[12] M. F. M. Arani and Y. A.-R. I. Mohamed, "Assessment and enhancement of a full-scale PMSG-based wind power generator performance under faults," *IEEE Trans. Energy Convers.*, vol. 31, no. 2, pp. 728–739, Jun. 2016.

[13] D. Xie, Y. Lu, J. Sun, and C. Gu, "Small signal stability analysis for different types of PMSGs connected to the grid," *Renew. Energy*, vol. 106, pp. 149–164, Jun. 2017.

[14] F. Zhang, S. Yu, Y. Wang, S. Jin, and M. G. Jovanovic, "Design and performance comparisons of brushless doubly fed generators with different rotor structures," *IEEE Trans. Ind. Electron.*, vol. 66, no. 1, pp. 631–640, Jan. 2019.

[15] Y. Cheng, B. Yu, C. Kan, and X. Wang, "Design and performance study of a brushless doubly fed generator based on differential modulation," *IEEE Trans. Ind. Electron.*, vol. 67, no. 12, pp. 10024–10034, Dec. 2020.

[16] T. D. Strous, H. Polinder, and J. A. Ferreira, "Brushless doubly-fed induction machines for wind turbines: Developments and research challenges," *IET Elect. Power Appl.*, vol. 11, no. 6, pp. 991–1000, Jul. 2017.

[17] Z. O. Yonah, A. M. El-Serafi, and A. E. Krause, "Computer-controlled VSCF generating system using a dual-excited synchronous generator," in *Proc. IEEE Pacific Rim Conf. Commun., Comput., Signal Process.*, May 1995, pp. 619–622.

[18] M. S. Morsy, H. H. Amer, M. A. Badr, and A. M. El-Serafi, "Transient stability of synchronous generators with two-axis slip frequency excitation," *IEEE Trans. Power App. Syst.*, vol. PAS-102, no. 4, pp. 852–859, Apr. 1983.

[19] M. Cheng, W. Hua, J. Zhang, and W. Zhao, "Overview of stator-permanent magnet brushless machines," *IEEE Trans. Ind. Electron.*, vol. 58, no. 11, pp. 5087–5101, Nov. 2011.

[20] A. B. Kjaer, S. Korsgaard, S. S. Nielsen, L. Demsa, and P. O. Rasmussen, "Design, fabrication, test, and benchmark of a magnetically geared permanent magnet generator for wind power generation," *IEEE Trans. Energy Convers.*, vol. 35, no. 1, pp. 24–32, Mar. 2020.

[21] Q. Wang and S. Niu, "Design, modeling, and control of a novel hybrid-excited flux-bidirectional-modulated generator-based wind power generation system," *IEEE Trans. Power Electron.*, vol. 33, no. 4, pp. 3086–3096, Apr. 2018.

[22] H. A. Moussa, M. A. Badr, and A. M. El-Serafi, "Power system damping enhancement by two-axis supplementary control of synchronous generators," *IEEE Trans. Power App. Syst.*, vol. PAS-104, no. 5, pp. 997–1004, May 1985.

[23] A. El-serafi and M. Badr, "Extension of the under-excited stable region of the dual-excited synchronous machine," *IEEE Trans. Power App. Syst.*, vol. PAS-92, no. 1, pp. 287–294, Jan. 1973.
[24] P. Subramaniam and O. P. Malik, "Dynamic-stability analysis of dwr synchronous generator with feedback-stabilised voltage and angle regulators," *Proc. Inst. Elect. Eng.*, vol. 118, no. 12, pp. 1768–1774, Dec. 1971.
[25] A. A. Reddy, S. S. Bhat, and R. T. Ugale, "Design and FEM analysis of dual excited synchronous generator," in *Proc. Nat. Power Electron. Conf. (NPEC)*, Dec. 2017, pp. 302–306.
[26] G. Xu, Z. Wang, B. Liu, Y. Zhan, W. Li, H. Zhao, H. Huang, and H. Yu, "Finite-element calculation of electromagnetic characteristics and steady-state stability of dual-excited synchronous generator," *IET Electr. Power Appl.*, vol. 15, no. 10, pp. 1300–1313, Oct. 2021.
[27] G. Xu, Y. Hu, X. Hao, Y. Zhan, H. Zhao, X. Liu, and Y. Luo, "The relationship of magnetomotive force under different excitation modes of dual-excited synchronous generator," *IEEE Trans. Magn.*, vol. 54, no. 3, pp. 1–4, Mar. 2018.
[28] Z. O. Yonah, A. M. El-Serafi, and A. E. Krause, "Regulation of terminal voltage and output frequency of a variable-speed dual-excited synchronous generator by using a computer-based two-phase excitation system," in *Proc. Can. Conf. Electr. Comput. Eng.*, Sep. 1993, pp. 1165–1168.
[29] L. Piegari, R. Rizzo, and P. Tricoli, "High efficiency wind generators with variable speed dual-excited synchronous machines," in *Proc. Int. Conf. Clean Electr. Power*, May 2007, pp. 795–800.
[30] S. D'Arco, L. Piegari, and P. Tricoli, "A novel control of dual-excited synchronous machines for variable-speed wind turbines," in *Proc. IEEE Trondheim PowerTech*, Jun. 2011, pp. 1–6.
[31] Z. O. Yonah, A. M. El-Serafi, and A. E. Krause, "Performance of a computer-based two-phase excitation system for a variable-speed dual-excited synchronous generator," in *Proc. IEEE WESCANEX Commun., Comput. Power Modern Environ. Conf.*, May 1993, pp. 263–268.
[32] R. R. Abdel-Wahab, H. M. Yassin, and H. H. Hanafy, "Dual excited synchronous generator a suitable alternative for wind applications," in *Proc. IEEE 14th Int. Conf. Compat., Power Electron. Power Eng. (CPE-POWERENG)*, Jul. 2020, pp. 352–357.

**H. M. YASSIN** received the B.Sc., M.Sc., and Ph.D. degrees in electrical power engineering from the Faculty of Engineering, Cairo University, Giza, Egypt, in 2007, 2011, and 2016, respectively. He is currently an Assistant Professor with the Electrical Power Engineering Department, Faculty of Engineering, Cairo University. His research interests include renewable energy systems, electric drives systems, and electric machines.

**R. R. ABDEL-WAHAB** was born in Egypt, in 1988. He received the B.Sc. and M.Sc. degrees in electrical power engineering from Cairo University, Egypt, in 2011 and 2017, respectively, where he is currently pursuing the Ph.D. degree. From 2013 to 2017, he was a Teaching Assistant with the Electrical Power Engineering Department, Faculty of Engineering, Cairo University, where he has been an Assistant Lecturer, since 2017. His research interests include electrical motors, electrical drives, wind energy conversion systems, and engineering education.

**H. H. HANAFY** received the B.Sc., M.Sc., and Ph.D. degrees (Hons.) in electrical power engineering from the Faculty of Engineering, Cairo University, Giza, Egypt, in 1992, 1997, and 2003, respectively. He is currently an Associate Professor with the Electrical Power Engineering Department, Faculty of Engineering, Cairo University. He is the author or coauthor of many refereed journals and conference papers. His research interests include electric machines, electric drives systems, electromagnetism, and wind energy systems.